
RAPID DETECTION AND RECOGNITION OF WHOLE BRAIN ACTIVITY IN A FREELY BEHAVING *Caenorhabditis elegans*

A PREPRINT

Yuxiang Wu

University of Science and Technology of China
elephantameler@mail.ustc.edu.cn

Shang Wu

University of Science and Technology of China
ws166@mail.ustc.edu.cn

Xin Wang

Shanghai Jiao Tong University

Chengtian Lang

University of Science and Technology of China

Quanshi Zhang

Shanghai Jiao Tong University

Quan Wen

University of Science and Technology of China
qwen@ustc.edu.cn

Tianqi Xu

University of Science and Technology of China
xutq@ustc.edu.cn

September 24, 2021

ABSTRACT

Advanced volumetric imaging methods and genetically encoded activity indicators have permitted a comprehensive characterization of whole brain activity at single neuron resolution in *Caenorhabditis elegans*. The constant motion and deformation of the mollusc nervous system, however, impose a great challenge for a consistent identification of densely packed neurons in a behaving animal. Here, we propose a cascade solution for long-term and rapid recognition of head ganglion neurons in a freely moving *C. elegans*. First, potential neuronal regions from a stack of fluorescence images are detected by a deep learning algorithm. Second, 2 dimensional neuronal regions are fused into 3 dimensional neuron entities. Third, by exploiting the neuronal density distribution surrounding a neuron and relative positional information between neurons, a multi-class artificial neural network transforms engineered neuronal feature vectors into digital neuronal identities. Under the constraint of a small number (20-40 volumes) of training samples, our bottom-up approach is able to process each volume - $1024 \times 1024 \times 18$ in voxels - in less than 1 second and achieves an accuracy of 91% in neuronal detection and 74% in neuronal recognition. Our work represents an important development towards a rapid and fully automated algorithm for decoding whole brain activity underlying natural animal behaviors.

1 Introduction

Characterizing whole-brain activity is crucial for opening the black box of a biological neural network. Recent technological advances in volumetric imaging, tracking, and genetically encoded calcium and voltage probes make it possible to simultaneously record the activity of a large fraction of neurons in a behaving animal (Nguyen et al. [2016], Venkatachalam et al. [2016], Cong et al. [2017], Kim et al. [2017], Aimon et al. [2019], Voleti et al. [2019], Peters et al. [2021], Zhang et al. [2021]), opening a window to exploration of brain dynamics and behaviors at multiple spatiotemporal scales.

Over time, constant deformation of a molluscan brain, which causes large displacement and distortion of a neuron, has been a major hindrance to rapid and accurate characterization of neural activity patterns. Furthermore, highly similar textures and shapes between neurons within an individual as well as highly variable distributions of neurons across individuals make detection and identification of neurons an extraordinarily challenging problem.

Extracting whole-brain activity from imaging data in a moving *C. elegans* requires answering two questions: *where are the neurons* and *who are they*. Conventional image processing methods and deep-learning-based methods have been proposed to solve both problems (Friedrich et al. [2017], Fürth et al. [2018], Giovannucci et al. [2019]). To answer the first question, traditional methods use explicit computational models to localize neuronal regions, for example, by computing the 3D Hessian matrix in the pixel space (Nguyen et al. [2017]) and by implementing watershed algorithm for regional segmentation (Wen et al. [2021] Nguyen et al. [2017] Couprie and Bertrand [1997]). Deep-learning-based methods, such as 3D-UNet (Çiçek et al. [2016] Wen et al. [2021]), train feed-forward neural network models to find candidate neuronal regions. With a sufficient number of human-annotated supervised examples, a neural network can effectively and accurately perform the neuron detection task.

Sequence-dependent and sequence-independent methods have been proposed to address the second question, namely to assign an identity to each neuron in every imaging volume. In a sequence-dependent method, a tracking or registration algorithm maps the correspondence between two sets of neurons in adjacent volumes, see for example Wen et al. [2021]. This method could work well for semi-immobilized *C. elegans* (Wen et al. [2021]), when cell displacements are relatively small and spatiotemporal continuity of imaging volumes approximately holds; but it is prone to error accumulation when cell displacements are large, rapid and not easily predictable.

Sequence-independent methods allocate neuron identities by ignoring the temporal order of imaging volumes. For example, by carefully designing a feature vector for each neuron in every volume, Nguyen et al. [2017] could allocate neuron identities all at once by a hierarchical clustering algorithm. In a different approach, an algorithm aims to find optimal neuron assignment by maximizing the intrinsic similarity between a point-set in a testing volume and that in a different imaging volume or in human-annotated atlases (e.g., OpenWorm Szigeti et al. [2014] or NeuroPAL Yemini et al. [2021]). The intrinsic similarity could be cast in a probabilistic graphic model (Chaudhary et al. [2021]) or a transformer neural network model (Yu et al. [2021]). Notably, these methods could also be used for identifying neurons across individuals.

With recent development in machine vision and deep learning, we are crying out for fast, efficient, and user-friendly algorithms that take, with minimum human interference, raw volumetric imaging data as inputs and extract neural activity traces from all recorded neurons. Unlike in immobilized animals where cell positions are invariant and spatiotemporal segmentation could be implemented at once (Cao et al. [2020], Greenwald et al. [2021]), 3D neuron detection and segmentation in freely behaving *C. elegans* is carried out in every imaging volume independently and has become the speed bottleneck (Nguyen et al. [2017], Wen et al. [2021]). To identify neurons across volumes, recent deep-learning-based models (Yu et al. [2021], Wen et al. [2021]) require enormous training samples (e.g., large computer-generated synthetic datasets) or specialized processing steps such as straightening a worm (Wen et al. [2021]) to facilitate neuron mapping and error corrections. Despite the presence of modern gadgets, it remains challenging for a machine to approach a recognition accuracy matching human annotation.

Here, we propose a streamlined approach, called CenDr (*C. elegans* **n**euron **D**etection and **r**ecognition), to extract whole brain neural activity patterns in a freely behaving *C. elegans*. As in previous works (Nguyen et al. [2016] Venkatachalam et al. [2016]), we combine a spinning disk confocal microscope and a customized tracking system to record neural activity in the head ganglion while the animal is moving. We use nuclei-localized red fluorescent protein (mNeptune) as a reference channel to localize and recognize neurons. The CenDr system processes an imaging volume in the following 4 steps. 1) An automatic pre-processing procedure segments the head region and build a *C. elegans* coordinate system. 2) A multi-field detection (MFD) neural network finds, with high confidence, a set of neuronal regions on each frame in a volume. 3) By treating regional alignment across adjacent frames as a maximum bipartite matching problem, we use the Hungarian method to merge candidate regions into a neuron. 4) A multi-class recognition neural network assigns an id to every neuron in a random volume using two input feature vectors, designed to extract neuronal density and relative positional information surrounding a neuron. Our results show that with a few human-annotated examples, CenDr is able to rapidly identify whole brain neural activity with an accuracy that is comparable to contemporary methods.

2 Methodology

The CenDr pipeline (Fig. 1) takes a volume of size $W \times H \times F$ as an input (Fig. 1A), and outputs neuron objects including each neuron’s digital identity, location, and shape. Our approach comprises the following four steps. First, we use a combination of image processing algorithms to extract head and body regions and build the *C. elegans* coordinate

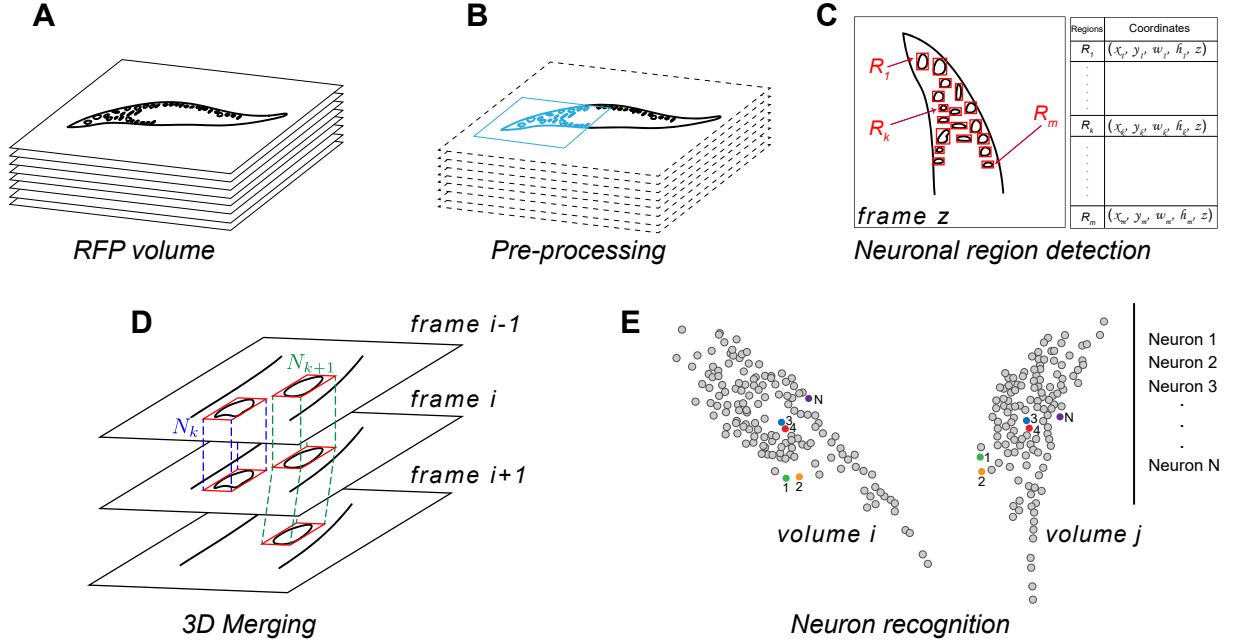


Figure 1: The CenDr pipeline. (A) A red channel (RFP) imaging volume consists of a stack of fluorescence images ($1024 \times 1024 \times 18$, see Section 3 for further details). (B) An Automatic Pre-Processing (APP) algorithm crops the head region (blue rectangle) and defines the *C. elegans* coordinate system. (C) A Multi-Field Detection (MFD) algorithm generates anchors of different sizes centered at local maxima of pixel intensities. An ANN refines the shapes and locations of anchors and proposes neuronal regions R (red rectangle) in every frame, each of which is represented by a quintuple (x, y, w, h, z) . (D) A 3D merging procedure views regional alignment across adjacent frames as a maximum bipartite matching problem, which can be solved by the Hungarian method. N_k and N_{k+1} illustrate how the procedure merges neuronal regions into two neuron objects. (E) A multi-class recognition neural network takes designed feature vectors and assigns an digital identity to every neuron in a volume. Neurons sharing the same identity are represented by the same color. N is the number of neurons to be recognized.

system for every volume (Fig. 1B). Second, we identify local pixel intensity maxima in a frame, which will be used as anchor points to build multi-field inputs. A trained neural network takes the inputs and predicts the score of each region as well as its position and shape. By removing overlaps between regions, the algorithm then finds a list of neuronal regions in every frame $\{R_1, R_2, R_3, \dots\}$ (Fig. 1C). Third, $\{R_k\}$ are appropriately merged into a set of neuron objects $\{\mathcal{N}_i | i \in \{1, \dots, N\}\}$ by the *NeuroAlignment* algorithm (Fig. 1D), where N is the total number of neurons in a volume. Finally, we engineer two feature vectors to characterize each neuron’s relationship with its surroundings. The concatenated features are transformed by a feed-forward recognition network into a set of digital identities i , where $i \in \{1, 2, 3, \dots\}$, which is unified across imaging volumes (Fig. 1E).

2.1 Stage 1: Pre-processing

We design an Automatic Pre-Processing (APP) algorithm to extract a head region and use it to build a *C. elegans* coordinate system (Fig. 2). We take the maximum intensity projection image I_{MIP} of each volume (Fig. 2B), denoise the image with median blur (Fig. 2C), and perform the morphological open operation - dilation followed by erosion - to find connected regions. Empirically, the size of the dilation filter is slightly bigger than the erosion filter. I_{MIP} is converted into a binary image using the dynamic threshold algorithm (Fig. 2D), and the contour tracing algorithm Bradski [2000] is conducted to find contour points $\{C_{head}\}$ of the head, namely the region with the maximal area (Fig. 2E). To build the *C. elegans* coordinate system, we calculate the *anterior* – *posterior* axis and *ventral* – *dorsal* axis intrinsic to a worm (see Algorithm 1). Later, all neuronal positions will be transformed into their intrinsic coordinates (see Section 3).

Algorithm 1 An algorithm to build the *C. elegans* coordinate system

Require: the head region I_{head} in the maximum intensity projection image I_{MIP} . Contour of the head $\{C_{head}\}$.

Ensure: center of mass O , anterior endpoint P_a , posterior endpoint P_p , ventral endpoint P_v and dorsal endpoint P_d .

- 1: We define a point of interest whose pixel value $\geq \bar{I}_{head} + \sigma(I_{head})$, namely the sum of standard deviation and mean of I_{head} . These selected points are used to compute moments and O .
- 2: $M_{00} = \sum_{x,y} I_{head}(x, y)$
- 3: $M_{10} = \sum_{x,y} x \cdot I_{head}(x, y)$, $M_{01} = \sum_{x,y} y \cdot I_{head}(x, y)$
- 4: $O \leftarrow (\frac{M_{10}}{M_{00}}, \frac{M_{01}}{M_{00}})$
- 5: O is the origin. The longest line segment passing O and intersecting $\{C_{head}\}$ at (P_a, P_p) defines the *anterior – posterior* axis.
- 6: The line segment perpendicular to the *anterior – posterior* axis defines the *ventral – dorsal* axis. It passes O and intersects $\{C_{head}\}$ at (P_v, P_d) .
- 7: The *ventral – dorsal* axis divides the head into two regions; the region containing a greater number of points of interest defines the *anterior* direction.
- 8: The *anterior – posterior* axis divides the head into two regions; the region containing a greater number of points of interest defines the *ventral* direction.

2.2 Stage 2: Neuronal region detection

In the second stage, we apply a deep learning algorithm to search for, frame by frame, all regions $\{R_k\}$ that belong to neurons. Each neuronal region is a rectangular bounding box, represented by a quintuple: $R_k = (x, y, w, h, z)$, where x and y are upper left coordinates of the rectangle; z is the frame index; w and h are width and height of the rectangle respectively.

Instead of examining each pixel in a frame, the APP algorithm from stage 1 has helped reduce the searching area to the head region (Fig.3A), which is much smaller than the size of an entire image. To further accelerate neuronal detection, we first identify local pixel intensity maxima in the head region (Fig. 3B). These local peaks $\{P_k\}$ likely belong to potential neuronal regions. The center and the size of a candidate region, however, remain unknown. Next, an Artificial Neural Network (ANN) is trained to obtain these information. The inputs to the ANN includes multiple rectangular bounding boxes centered at $\{P_k\}$, called anchors (Fig. 3C) and represented by $A = (x_A, y_A, w_A, h_A)$, where x_A and y_A are upper left coordinates of an anchor; w_A and h_A are width and height respectively. Multiple anchors of different sizes are used to cover neurons of various shapes. Multi-field images (Fig. 3D), which are concentric with the anchor, provide additional local and context information to the neural network. The ANN predicts a score S for each region, as well as the regional position and size, formulated as corrections, $(\Delta\hat{x}, \Delta\hat{y}, \Delta\hat{w}, \Delta\hat{h})$, to the anchor parameters (see Eq. 7). Finally, a non-maximum suppression algorithm ranks each potential neuronal region based on its score S , removes regional overlaps, and generates a set of neuronal regions $\{R_k\}$.

2.3 Stage 3: 3D merging

In the third stage, we introduce $\mathfrak{X}NeuroAlignment$ (Fig. 4) to merge $\{R_k^z\}$ that belong to the same neuron. We introduce the superscript $z \in \{1 \dots F\}$ to denote the frame index of a neuronal region. The continuous and sometimes irregular movements of a worm could lead to considerable shifts of $\{R_k^z\} \subseteq \mathcal{N}_i$ (Fig. 4A), a major challenge for achieving accurate alignment. In general, stage 2 could be viewed as a maximum weight matching problem in a graph: each $\{R_k^z\}$ is represented by a vertex; vertices belonging to the same neuron are connected by an edge whose weight is determined by the overlap between the two neuronal regions (see Eq. 2). This computationally intensive problem is significantly simplified by the following two observations.

- **Exclusion Principle:** each neuron appears at most once in a frame. All vertices representing $\{R_k^z\}$ with identical z value are disconnected.
- **Continuum Principle:** each neuron appears in only one frame or in consecutive frames. Other scenarios are forbidden. When a neuron appears in adjacent frames, an edge E is defined to connect two neuronal regions: $E \subseteq \{(R_m^z, R_n^{z+1}) \mid z \in \{1 \dots F-1\}, m \in \{1 \dots M_z\}, n \in \{1 \dots M_{z+1}\}\}$, where M_z is the number of neuronal regions in the z th frame.

Therefore, the combinatorial optimization problem is reduced to finding a set of edges $\{E\}$ that maximize the total weights \mathcal{W} in a chain of bipartite graphs:

$$\operatorname{argmax}_{\{E\}} \mathcal{W} = \sum_{z=1}^{F-1} \operatorname{argmax}_{\{E^{z,z+1}\}} \mathcal{W}^{z,z+1}, \quad (1)$$

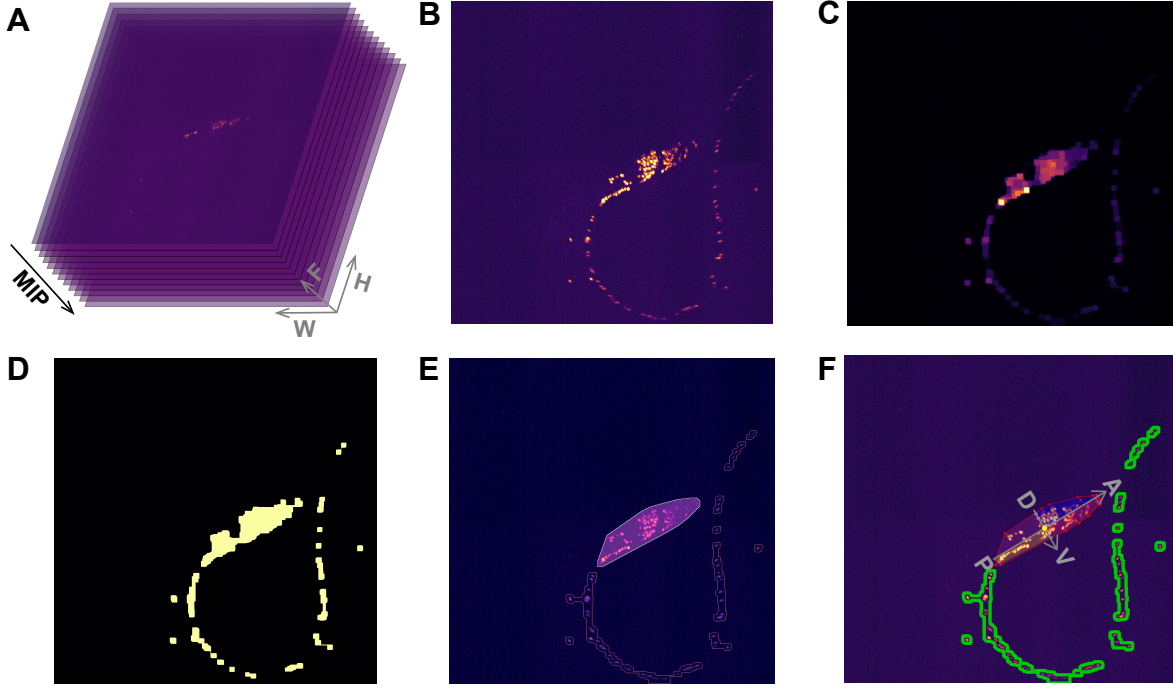


Figure 2: **Automatic Pre-Processing (APP).** (A) An RFP imaging volume. (B) Maximum Intensity Projection (MIP) of the imaging volume. Brighter pixels represent fluorescence signals. (C) Noises are reduced by median blur filters; an open operation followed by an extra dilation connect neighboring pixels, from which the worm head region will be extracted. (D) A dynamic threshold algorithm converts (C) into a binary image. (E) A contour finding algorithm identifies a series of separate regions. The largest area (yellow contour with a purple mask) is the head region; the rest are body regions (pink contour). (F) A *C. elegans* coordinate system is built for the head region. The yellow point represents the center of mass. A: anterior, P: posterior, V: ventral and D: dorsal.

where $\mathcal{W}^{z,z+1}, \{E^{z,z+1}\}$ are total weights and edges in a bipartite graph connecting vertices from adjacent frames. Because each neuronal region belongs to only one neuron, Eq. 1 is subject to the constraint that $\{E^{z,z+1}\}$ should not share a common vertex. In other words, the entire graph is a linked list (Fig. 4B1), not a tree.

We now define the weight of an edge (R_m^z, R_n^{z+1}) using the Intersection over Union (abbr. IoU),

$$w(R_m^z, R_n^{z+1}) = \frac{R_m^z \cap R_n^{z+1}}{R_m^z \cup R_n^{z+1}}, \quad (2)$$

which quantifies the regional overlap. Eqs. (1-2) can be solved by the Hungarian algorithm (Fig. 4B2). Note that all $w(R_m^z, R_n^{z+1}) < \tau$ are set to 0, where $\tau = 0.05$ is a predefined IoU threshold.

The Hungarian algorithm will accidentally merge two neighboring neurons along the z axis. We design a partition method to resolve this problem. First, we compute the mean pixel intensity of every neuronal region R_k in a neuron \mathcal{N}_i . Second, if the distribution of pixel intensity across frames is multi-modal, we will split \mathcal{N}_i at the z th frame if the mean pixel intensity of R_k^z is minimal (Fig. 4B3).

2.4 Stage 4: Neuron recognition

In the final stage, we propose a few-shot learning method to recognize the digital identity of each neuron. Here, we face two major challenges. First, a typical neuron in our imaging volume does not possess a distinct texture or shape, and the disparity in the appearances of the same neuron across volumes can be even bigger than those between different neurons (Fig.5A). Second, the location of a neuron is constantly changing. What remains to be invariant and distinct is

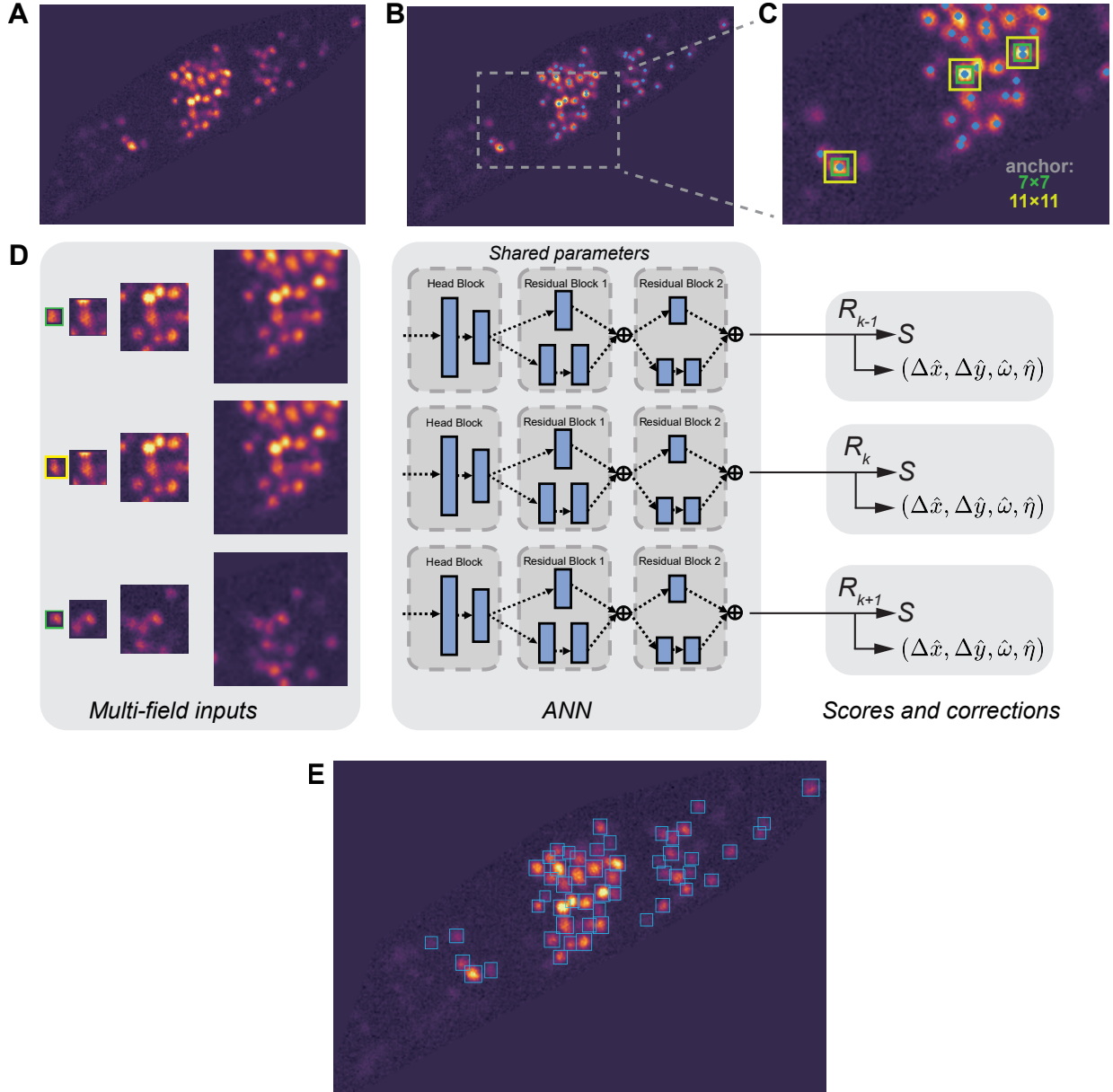


Figure 3: **Multi-Field Detection (MFD).** (A) A cropped head region. Every frame in a volume is cropped in the same way. (B) Find local pixel intensity maxima (blue points) in A. (C) An enlarged view of the rectangular region in (B). 6 anchors of different sizes are centered at 3 local maxima. The green or yellow rectangle represents a 7×7 or 11×11 anchor. (D) An Artificial Neural Network (ANN) including residual blocks receives multi-field inputs once at a time and outputs a score S and corrections $(\Delta\hat{x}, \Delta\hat{y}, \Delta\hat{\omega}, \Delta\hat{\eta})$ to the position and shape of an input anchor. The green anchor (first row) and the yellow anchor (second row) have the same center but different sizes; the green anchors in the first and third row have the same size but different centers. The four multi-field images in a row are concentric. The score S infers the probability of an anchor being a neuronal region; the corrections refine the shape and location of an anchor. (E) A detection result. Refined anchors centered at local pixel intensity maxima are filtered by a non-maximum suppression algorithm. Blue rectangles are detected neuronal regions.

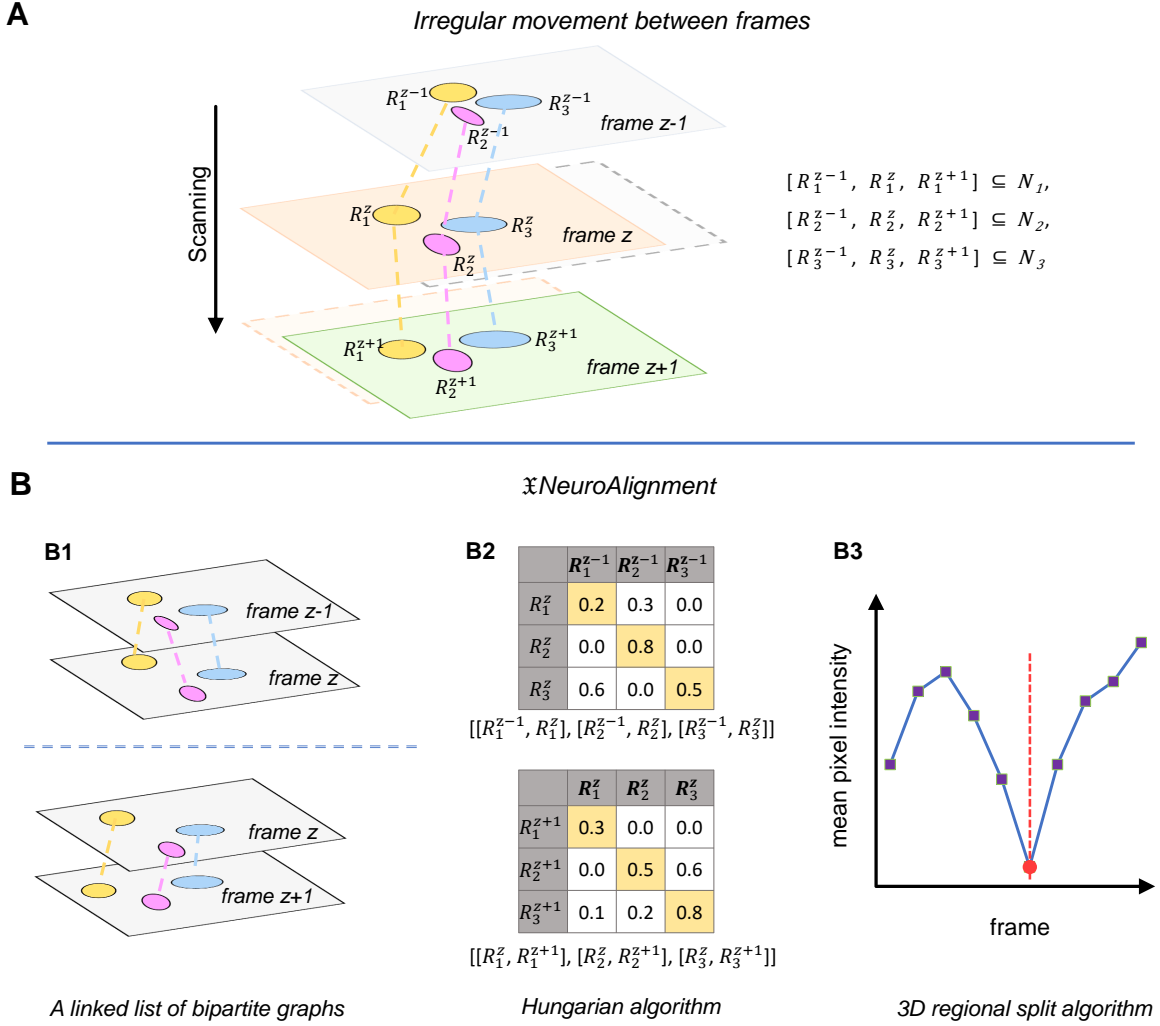


Figure 4: 3D merging. (A) An illustration of irregular cell movements across frames. The problem of regional alignment arises when the movements of neurons are significant during a single z -scan of the imaging volume. Regions belonging to the same neuron, which are represented by ellipses with an identical color, could display considerable displacements between frames. (B) The *NeuroAlignment* algorithm for 3D merging. B1, the algorithm views neuronal regions in a volume as vertices in a linked list of bipartite graphs, where the IoU score between neuronal regions is the weight of an edge. B2, every possible alignment between adjacent frames can be represented by a weight matrix, and the Hungarian algorithm is used to find an optimal row and column permutation that maximizes the trace (yellow color) of the matrix. B3, a 3D regional split algorithm (right) calculates the mean pixel intensity distribution of a neuronal region across all the frames in a neuron. If the distribution is multi-modal, the algorithm will split one neuron object into two at the local minimum (red vertical line).

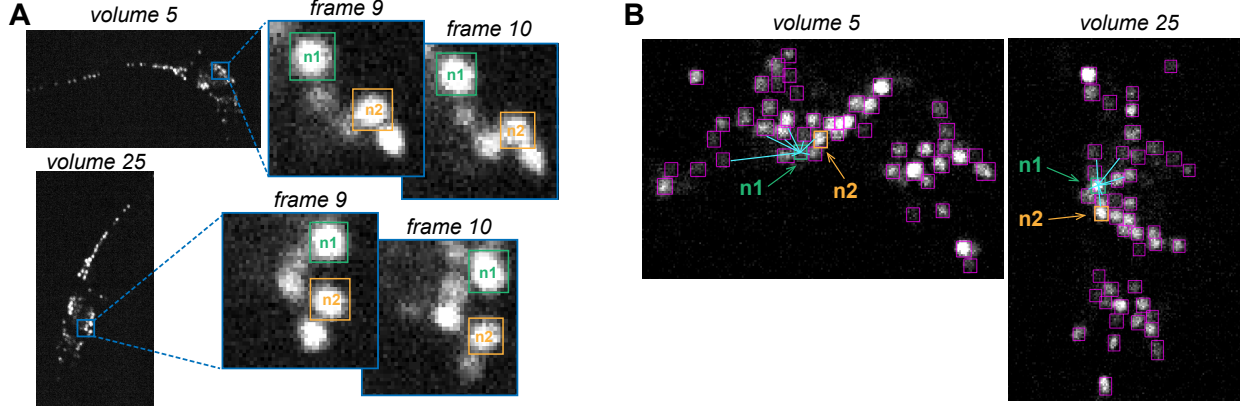


Figure 5: **A neuron’s relative position is a more discriminable feature than its shape and texture.** (A) The shape or texture of a neuron in an imaging volume is not a distinct feature, which varies significantly across volumes. (B) The position of a neuron relative to its neighboring partners is a more robust and discriminable feature. For example, neuron $n1$ and $n2$ display similar relative positions in volumes 5 and 25.

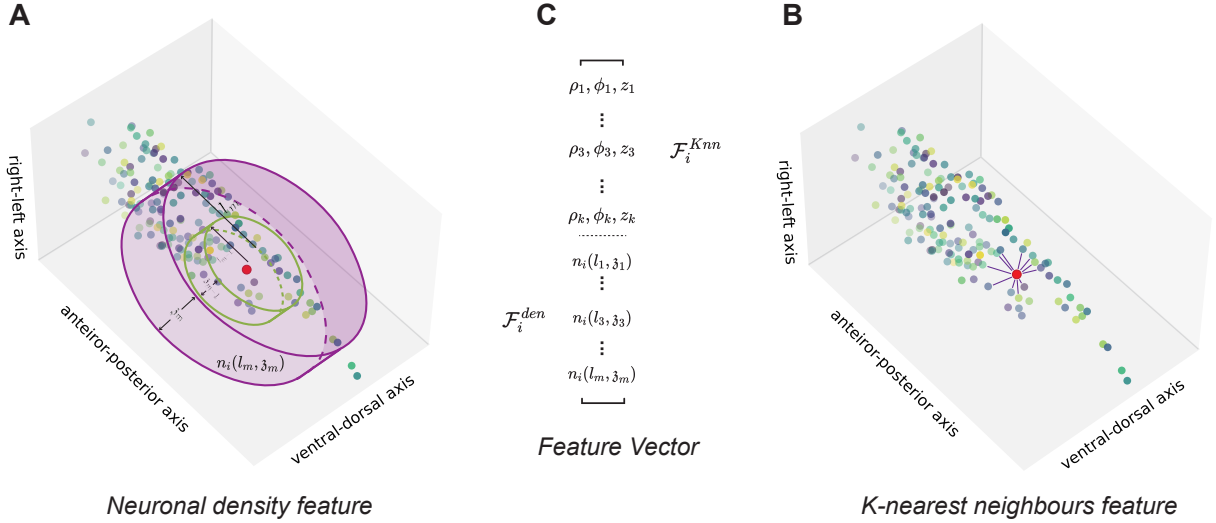


Figure 6: **Construction of feature vectors for recognizing digital identities of *C. elegans* neurons.** A 3-dimensional atlas of all detected neurons in a *C. elegans* head region. The red point assigns neuron \mathcal{N}_i as the origin in the *C. elegans* coordinate system. (A) The neuronal density feature is constructed by counting the number of neurons n between two color-coded concentric cylinders with expanding radii l and heights z . (B) Radiating lines connect \mathcal{N}_i with its K -nearest neighbours, whose coordinates are used as positional features. (C) The recognition feature vector is constructed by concatenating \mathcal{F}_i^{den} in (A) and \mathcal{F}_i^{Knn} in (B).

a neuron’s position relative to its surroundings (Fig.5B). We, therefore, propose two discriminable features based on density distribution surrounding a neuron and each neuron’s K -nearest neighbors.

In this section, we shall ignore the size of a neuron object by treating it as a point in 3 dimensions. We shall use the *C. elegans* coordinate system where neuron \mathcal{N}_i is the origin.

Neuronal density feature Formally, we introduce the neuronal density function at a position $\mathbf{x} = [x, y, z]$ using the Dirac δ function

$$g_i(\mathbf{x}) = \sum_{j \neq i} \delta(\mathbf{x} - \mathbf{x}_j), \quad (3)$$

\mathbf{x}_j is the position of neuron j in our imaging volume, and by definition, $\mathbf{x}_i = [0, 0, 0]$. We can understand the physical meaning of $g(\mathbf{x})$ by integrating Eq. 3 over a small volume $d^3\mathbf{x}$ at a separation \mathbf{x} from the origin, which gives the number of neurons in that small volume. $g_i(\mathbf{x})$ is also called pair correlation function in statistical physics. We introduce the subscript i to emphasize the fact that $g_i(\mathbf{x})$ is a different function when a different neuron \mathcal{N}_i is centered at the origin of the *C. elegans* coordinate system.

Next, we replace \mathbf{x} by the cylindrical coordinate $[\rho, \phi, z]$ and count the number of neurons *in between* two cylinders, one of which is described by height and radius parameters (\mathfrak{z}, l) , and the other is described by $(\mathfrak{z} - \Delta\mathfrak{z}, l - \Delta l)$ (Fig. 6A):

$$n_i(l, \mathfrak{z}) = \int_{-\mathfrak{z}/2}^{\mathfrak{z}/2} dz \int_0^l \rho d\rho \int_0^{2\pi} d\phi g_i(\rho, \phi, z) - \int_{-(\mathfrak{z}-\Delta\mathfrak{z})/2}^{(\mathfrak{z}-\Delta\mathfrak{z})/2} dz \int_0^{l-\Delta l} \rho d\rho \int_0^{2\pi} d\phi g_i(\rho, \phi, z), \quad (4)$$

The neuron density feature is a vector $\mathcal{F}_i^{den} = [n_i(l_1, \mathfrak{z}_1), \dots, n_i(l_m, \mathfrak{z}_m)]$, where l_m and \mathfrak{z}_m are discretized quantities for l and \mathfrak{z} .

K-nearest neighbor feature The cylindrical coordinates $[\rho, \phi, z]$ of K-nearest neurons surrounding \mathcal{N}_i are used to build the K-nearest neighbor feature vector (see Fig. 6B): $\mathcal{F}_i^{Knn} = [\rho_1, \phi_1, z_1, \dots, \rho_K, \phi_K, z_K]$. The K neurons are arranged in an ascending order based on their distance from the origin.

We build \mathcal{F}^{den} and \mathcal{F}^{Knn} for all neurons $\{\mathcal{N}_i | i \in \{1, \dots, N\}\}$ in a random volume and then train an ANN classifier to predict their digital identities.

3 CenDr system

The CenDr system takes raw volumetric imaging data from a freely behaving *C. elegans* and extracts neural activity from all recorded neurons.

3.1 Imaging setup

To capture whole brain neural activity in a freely behaving *C. elegans*, we combined a spinning disk confocal inverted microscopy (Nikon Ti-U and Yokogawa CSU-W1, Japan) with a customized upright light path for worm tracking. Fluorescence signals, emitted from neurons at different depths in the worm head ganglion, were collected by a high NA objective (40X, NA = 0.95, Nikon Plan Apo, or 60X, NA = 1.20, Nikon Plan Apo WI), driven by a high-precision scanner (PI P721.CDQ) at a 5-Hz volume rate. An imaging volume comprises 18 two-channel fluorescence images recorded at 100 fps by two sCMOS cameras (Andor Zyla 4.2, England) simultaneously. A customized infrared LED ring (750 nm) was mounted above a worm, and dark-field images of worm behaviors were captured by the upright light path and recorded at 25 fps by a USB-3.0 camera (Basler acA2000-165umNIR).

3.2 Red fluorescence channel for detecting and identifying neurons

Our calcium imaging experiments were carried out on transgenic animals (*Pregf-1::GCaMP6::3*NLS::mNeptune*, *hpls676*, *ZM9644*), where green fluorescent calcium indicator GCaMP and red fluorescent protein mNeptune are co-expressed in the cell nuclei by a pan-neuronal promoter. The activity-independent RFP channel was used to detect and identify a neuron; the activity-dependent signal was extracted by linearly mapping the neuron position from the red to the green channel (Figure 7). We inferred neural activity from the ratiometric measure:

$$\mathfrak{R} = \frac{F_{\text{GCaMP}}}{F_{\text{RFP}}}, \quad (5)$$

where the red fluorescence F_{RFP} was used as a reference to reduce spurious signals arising from animal movements.

4 Evaluation

We now evaluate the performance of our CenDr system. The first task involves localizing and identifying the shape of every neuron in a volume. We propose to use two F1 scores to quantify the performance of 2D neuron detection and 3D merging. The second task involves allocating an identity for every neuron in a volume, for which the top-1 and top-3 accuracy are calculated. We also present a detailed speed analysis of the pipeline.

4.1 Neuron detection

Neuron detection consists of two stages, 2D regional detection and 3D merging. We use precision, recall, and F1 score to quantify 2D and 3D results, respectively. We divided our imaging data into 40 training volumes, 4 validation volumes,

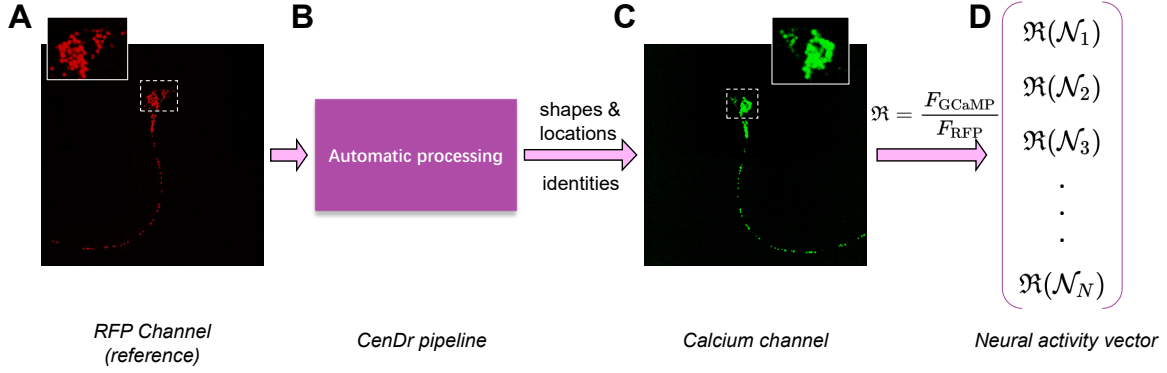


Figure 7: **The CenDr system.** (A) An RFP channel volume. (B) The CenDr pipeline takes the raw imaging data and outputs the location, shape and identity of every neuron in a volume. (C) A calibrated linear map allows the identification of each neuron’s location in the green channel, from which the calcium fluorescence signals, F_{GCaMP} of all recognized neurons can be extracted. (D) The whole-brain neural activity vector \mathfrak{R} can be inferred from the ratio of F_{GCaMP} to F_{RFP} .

and 26 test volumes. A model was saved if its performance on the validation volumes showed the best 2D F1 score during the training phase, see Table 1 for details. If the IoU (intersection over union) between a predicted region and a ground truth region is greater than a threshold 0.3, the predicted region is a True Positive (TP). Precision is the ratio of the number of TPs to the number of predicted regions, and recall is the ratio of TPs to the number of ground truth regions. F1 score is defined as the harmonic mean of precision and recall, namely $2/(\text{recall}^{-1} + \text{precision}^{-1})$.

Region correction. We use a simple location transform to implement region correction, inspired by Girshick et al. [2014]. During training, an ANN took an anchor region as an input and generated a score S , as well as corrections to the anchor position and size $(\Delta\hat{x}, \Delta\hat{y}, \hat{\omega}, \hat{\eta})$. The ground truth that has the maximum overlap with the anchor is the target. The ANN computed the binary cross-entropy loss for S and L2 loss for position and size corrections. The targeted corrections are defined as:

$$\begin{aligned}\Delta x &= (x_G - x_A)/w_A \\ \Delta y &= (y_G - y_A)/h_A \\ \omega &= w_G/w_A \\ \eta &= h_G/h_A\end{aligned}\tag{6}$$

where x_G, y_G, w_G, h_G represent upper left coordinates, width and height of a ground-truth (target) region; x_A, y_A, w_A, h_A represent upper left coordinates, width and height of an anchor. During inference, an anchor and its predicted corrections $(\Delta\hat{x}, \Delta\hat{y}, \hat{\omega}, \hat{\eta})$ were transformed into a neuronal region candidate (x, y, w, h) :

$$\begin{aligned}x &= \Delta\hat{x} \cdot w_A + x_A \\ y &= \Delta\hat{y} \cdot h_A + y_A \\ w &= \hat{\omega} \cdot w_A \\ h &= \hat{\eta} \cdot h_A\end{aligned}\tag{7}$$

ANN training. Our detection neural network was trained by 40 imaging volumes and 4 validation volumes. We used stochastic gradient descent with warm restarts and cosine annealing optimization strategy (Loshchilov and Hutter [2016]) to better optimize network parameters and avoid the gradient explosion situation. The ANN model took 5-channel 41×41 concentric multi-field images as inputs (Fig. 3D), including an anchor and 4 cropped images with various sizes ($15 \times 15, 31 \times 31, 41 \times 41, 81 \times 81$). Smaller or larger patch size would facilitate local or global feature learning respectively. A patch smaller than 41×41 was padded to 41×41 ; a patch bigger than 41×41 was resized to 41×41 . The APP algorithm later removed regions whose scores $S < 0.40$ and whose overlapping thresholds (derived from the non-maximum suppression algorithm) are less than 0.20. Table 1 presents performances from different anchor sizes, in which 9×9 provides the best trade-off between speed and accuracy.

4.2 Neuron recognition

Our recognition neural network was trained on 21 imaging volumes and 3 validation volumes. A model was saved if its performance has the best top-1 accuracy on validation volumes. Table 2 presents the model performance from 7 test

Table 1: **3D detection results.** Three experimental results are presented: 3D merging of human annotated neuronal regions, where 2D detection performance is irrelevant and thereby represented by "-"; 3D merging of neuronal regions detected an ANN, in which two different sets of predefined anchor sizes - "9x9" and "7x7, 11x11" - are used. The first row presents the performance of a single 3D merging algorithm. Although anchor sizes "7,11" have better 2D detection F1 score, this combination exhibits lower speed and F1 score in total 3D detection than anchor size "9". A different number of detected 2D regions could lead to a different 3D merging time. "ms/vol" refers to milliseconds per volume.

3D Detection								
Neuronal region detection					3D Merging			
Anchor size	Precision	Recall	F1 score	speed (ms/vol)	Precision	Recall	F1 score	speed (ms/vol)
-	-	-	-	-	97.63%	86.20%	91.55%	57
9	94.74%	95.75%	95.23%	791	91.51%	78.96%	84.77%	58
7,11	94.77%	96.30%	95.53%	1568	90.78%	78.04%	83.93%	61

Table 2: **Comparison among different neuronal identification methods in a freely moving *C. elegans*.** Here, we report accuracy and speed in different identification methods. "-" refers to the fact that no specific data is available; "s/vol" refers to seconds per volume. "Cross individuals" indicates whether a method can directly allocate identities across individual animals. The number of identities in a test set is abbreviated as "IDs". Accuracy includes top-1 accuracy and top-3 accuracy. Training dataset indicates the number of raw volumes or synthetic data, because 3DeeCellTracker (Wen et al. [2021]) and fDNC (Yu et al. [2021]) produce many synthetic samples to enhance method accuracy. 3DeeCellTracker tests their performance in a "straightened" animal, derived from a freely behaving *C. elegans* dataset (Nguyen et al. [2017]). Because 3DeeCellTracker only reported the speed of the entire pipeline, the number is the upper bound of its tracking time.

Name	Method	Training dataset (volumes)	State	Cross individuals	IDs	Accuracy	Speed (s/vol)
3DeeCellTracker (single mode)	tracking	1 / >500,000,000	straightened	false	90	73% / -	<73
3DeeCellTracker (ensemble mode)	tracking	1 / >500,000,000	straightened	false	90	99.8% / -	<86
fDNC	matching	4,000 / 230,400	freely moving	true	69.2	80.0% / -	0.01
our work	recognition	21 / 0	freely moving	true	134	74.17% / 93.54%	0.022

volumes. Note that the 7 test volumes are from the same worm. The performance across individuals will be presented in an updated version.

The recognition neural network receives two types of feature vectors from each neuron: a 150-dimensional (50×3) K-nearest neighbor feature vector and a 30-dimensional neuronal density feature vector. There are 133 neurons to be identified across volumes and an extra id that is not assigned to any neurons in the first place. Our designed feature vectors are intuitive. With a simple architecture and few training data, the recognition neural network can allocate 134 identities in ~ 20 ms at a 74.17% top-1 and 93.54% top-3 accuracy. The top-3 result is useful for human proofreading.

4.3 Speed analysis

We present, in Fig. 8, a detailed analysis of the processing time at each step in the CenDr pipeline. The two ANNs (detection and recognition neural networks) ran on a GeForce RTX 2080 Ti GPU (11 GiB, 11 TFLOPS in single precision) with CUDA 10.3, and other computations ran on an Intel E5-2678V3 CPU (12 Cores, 2.4 GHz). Our analysis excludes the time for data loading and results saving. CenDr is a highly-encapsulated and parallelized system that is able to process acquired volumes simultaneously (e.g., 341 volumes in 5.1 minutes).

5 Discussion

CenDr is able to rapidly detect and recognize neurons (< 1 sec/vol) from whole brain imaging data without compromising the accuracy (Table 1 and Table 2). If speed is a concern, our stage 2 and stage 3 in the pipeline provide an alternative to other neuron detection methods. For example, Wen et al. [2021] combines 3D-UNet (Çiçek et al. [2016]) and the watershed algorithm for cell segmentation, which relies heavily on 3D convolution and thereby could be slow.

The performance of our recognition model is also comparable to several other state-of-the-art methods. In their pioneering work, Nguyen et al. [2017] built a 300-dimensional feature vector for each neuron in every imaging volume by mapping its correspondence to a point set in each of the 300 reference volumes. This process used a non-rigid

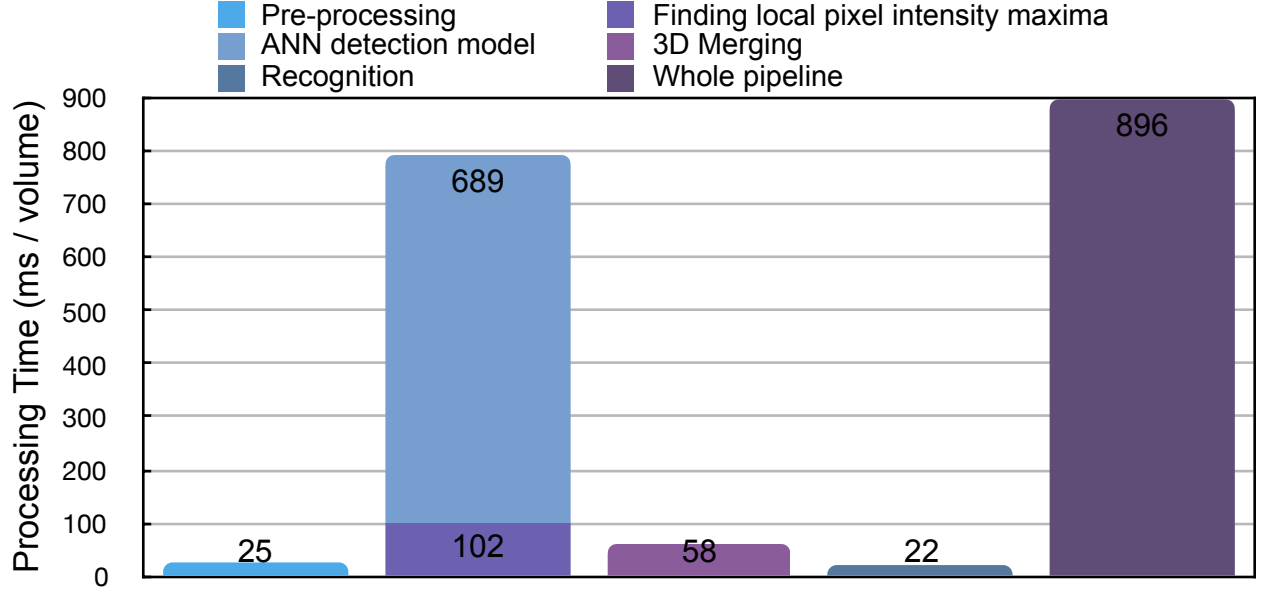


Figure 8: **Speed of the CenDr pipeline.** The processing time (ms/vol) of the entire pipeline and at each step are presented. The detection step consists of finding local pixel intensity maxima and an ANN detection model. The recognition step contains feature engineering (17 ms) and a multi-class ANN model (5 ms).

registration method and could be time-consuming. In another promising approach, Yu et al. [2021] trained a transformer neural network model (Vaswani et al. [2017]) to learn implicit neuronal features from a large synthetic dataset. The model could rapidly (~ 10 ms) infer a neuron’s identity in a test volume by computing the cosine similarity between the neuronal features and those in a template volume. It is also possible to explicitly model the joint probability distribution of neuron positions using conditional random field (CRF), and the neuron identity assignment is formulated as an optimization problem that can be solved by loopy belief propagation (Chaudhary et al. [2021]).

The accuracy of neuronal detection and recognition can be further improved by combining CenDr with newly developed genetic and imaging methods. For example, whole brain calcium imaging has been augmented by genetically sparse labeling neurons that can be seen in orthogonal color channels (Yemini et al. [2021]). These landmark neurons possess invariant identities and provide invaluable information for neuron identification across individuals (Yemini et al. [2021]). Within an individual, additional color information is also very helpful in the scenario of large brain deformation, namely when head movement causes a large group of neurons to be squeezed into a very small region.

CenDr is a versatile method for detecting and recognizing neurons and their activity in a freely behaving animal. When dealing with data collected under different experimental conditions (e.g., different imaging solutions and worm strains), CenDr aims to quickly learn the statistical representation of neurons and their relationships from a small number of human-annotated examples. We have also made an effort to minimize the number of parameters that need to be blindly tuned. Our supervised approach makes CenDr potentially applicable to a spectrum of volumetric imaging data, including neural activity recordings in other model organisms, such as *Drosophila* and zebrafish.

6 Acknowledgments

We thank Professor Mei Zhen for kindly providing us with the transgenic animal for whole brain imaging and Xiangyu Zhang for proof-reading some of the imaging volumes.

References

Jeffrey P Nguyen, Frederick B Shipley, Ashley N Linder, George S Plummer, Mochi Liu, Sagar U Setru, Joshua W Shae-vitz, and Andrew M Leifer. Whole-brain calcium imaging with cellular resolution in freely behaving *Caenorhabditis elegans*. *Proceedings of the National Academy of Sciences*, 113(8):E1074–E1081, 2016.

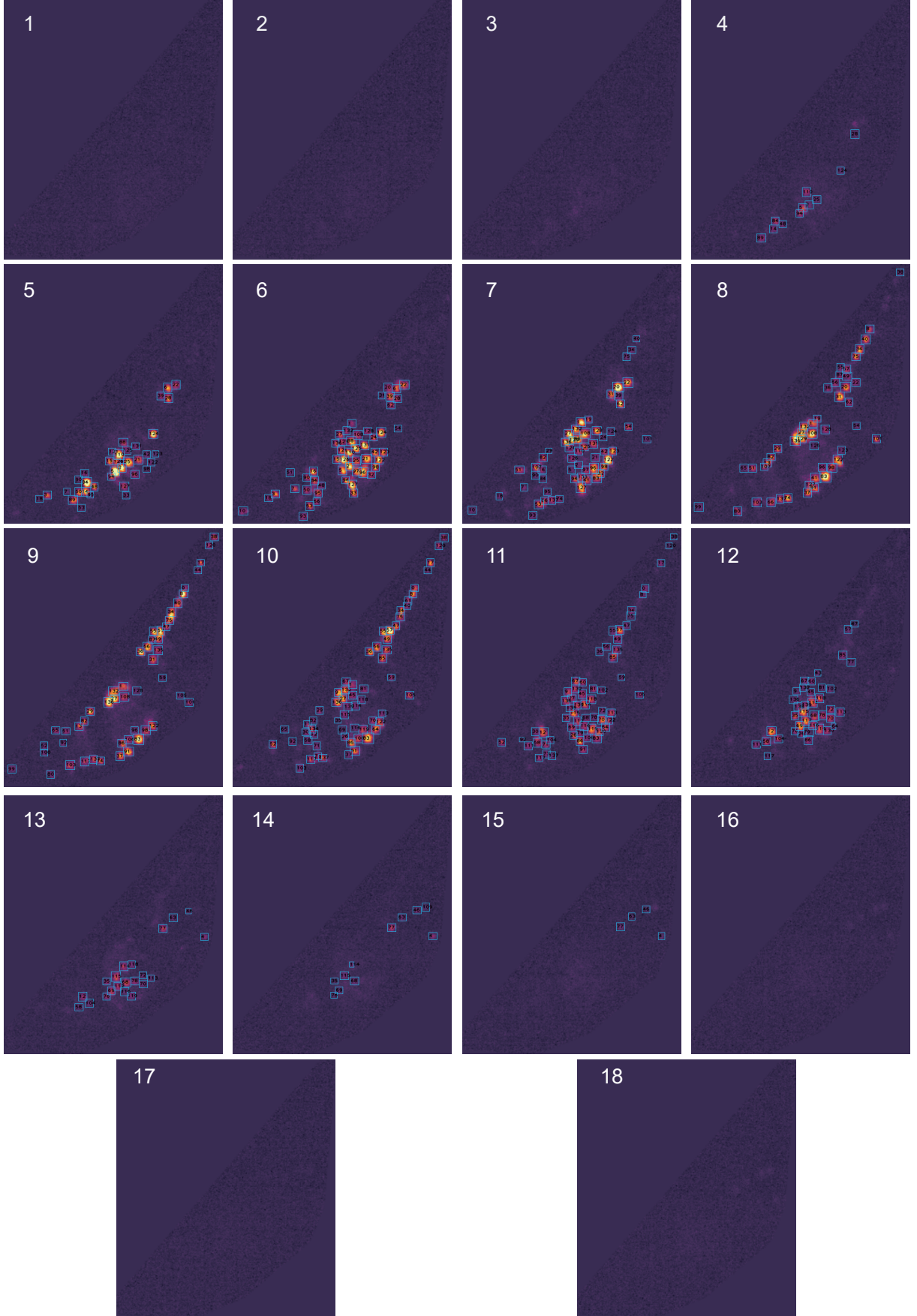


Figure 9: **Qualitative results.** Detection (blue rectangle) and recognition results (black number inside a blue rectangle). Note that a raw imaging volume ($1024 \times 1024 \times 18$) has been automatically cropped into a smaller size ($582 \times 470 \times 18$) that embeds a head region.

- Vivek Venkatachalam, Ni Ji, Xian Wang, Christopher Clark, James Kameron Mitchell, Mason Klein, Christopher J Tabone, Jeremy Florman, Hongfei Ji, Joel Greenwood, et al. Pan-neuronal imaging in roaming *Caenorhabditis elegans*. *Proceedings of the National Academy of Sciences*, 113(8):E1082–E1088, 2016.
- Lin Cong, Zeguan Wang, Yuming Chai, Wei Hang, Chunfeng Shang, Wenbin Yang, Lu Bai, Jiulin Du, Kai Wang, and Quan Wen. Rapid whole brain imaging of neural activity in freely behaving larval zebrafish (*Danio rerio*). *eLife*, 6:e28158, sep 2017. ISSN 2050-084X. doi:10.7554/eLife.28158. URL <https://doi.org/10.7554/eLife.28158>.
- Dal Hyung Kim, Jungsoo Kim, João C Marques, Abhinav Grama, David G C Hildebrand, Wenchao Gu, Jennifer M Li, and Drew N Robson. Pan-neuronal calcium imaging with cellular resolution in freely swimming zebrafish. *Nature Methods*, 14(11):1107–1114, 2017. ISSN 1548-7091. doi:10.1038/nmeth.4429.
- Sophie Aimon, Takeo Katsuki, Tongqiu Jia, Logan Grose, Michael Broxton, Karl Deisseroth, Terrence J. Sejnowski, and Ralph J. Greenspan. Fast near-whole-brain imaging in adult drosophila during responses to stimuli and behavior. *PLOS Biology*, 17(2):e2006732, 2019. ISSN 1544-9173. doi:10.1371/journal.pbio.2006732.
- Venkataushik Voleti, Kripa B. Patel, Wenze Li, Citlali Perez Campos, Srinidhi Bharadwaj, Hang Yu, Caitlin Ford, Malte J. Casper, Richard Wenwei Yan, Wenxuan Liang, and et al. Real-time volumetric microscopy of in vivo dynamics and large-scale samples with scape 2.0. *Nature Methods*, 16(10):1054–1062, 2019. ISSN 1548-7091. doi:10.1038/s41592-019-0579-4.
- Andrew J. Peters, Julie M. J. Fabre, Nicholas A. Steinmetz, Kenneth D. Harris, and Matteo Carandini. Striatal activity topographically reflects cortical activity. *Nature*, 591(7850):420–425, 2021. ISSN 0028-0836. doi:10.1038/s41586-020-03166-8.
- Zhenkun Zhang, Lu Bai, Lin Cong, Peng Yu, Tianlei Zhang, Wanzhuo Shi, Funing Li, Jiulin Du, and Kai Wang. Imaging volumetric dynamics at high speed in mouse and zebrafish brain with confocal light field microscopy. *Nature Biotechnology*, 39(1):74–83, 2021. ISSN 1087-0156. doi:10.1038/s41587-020-0628-7.
- Johannes Friedrich, Pengcheng Zhou, and Liam Paninski. Fast online deconvolution of calcium imaging data. *PLOS Computational Biology*, 13(3):e1005423, 2017. ISSN 1553-734X. doi:10.1371/journal.pcbi.1005423.
- Daniel Fürth, Thomas Vaissière, Ourania Tzortzi, Yang Xuan, Antje Martin, Iakovos Lazaridis, Giada Spigolon, Gilberto Fisone, Raju Tomer, Karl Deisseroth, et al. An interactive framework for whole-brain maps at cellular resolution. *Nature neuroscience*, 21(1):139–149, 2018.
- Andrea Giovannucci, Johannes Friedrich, Pat Gunn, Jérémie Kalfon, Brandon L Brown, Sue Ann Koay, Jiannis Taxis, Farzaneh Najafi, Jeffrey L Gauthier, Pengcheng Zhou, and et al. Caiman an open source tool for scalable calcium imaging data analysis. *eLife*, 8:e38173, 2019. doi:10.7554/elife.38173.
- Jeffrey P. Nguyen, Ashley N. Linder, George S. Plummer, Joshua W. Shaevitz, and Andrew M. Leifer. Automatically tracking neurons in a moving and deforming brain. *PLOS Computational Biology*, 13(5):e1005517, 2017. ISSN 1553-734X. doi:10.1371/journal.pcbi.1005517. require low-high mag straitening, which may be unaccurate when overlap them.
- Chentao Wen, Takuya Miura, Venkataushik Voleti, Kazushi Yamaguchi, Motosuke Tsutsumi, Kei Yamamoto, Kohei Otomo, Yukako Fujie, Takayuki Teramoto, Takeshi Ishihara, et al. 3deecelltracker, a deep learning-based pipeline for segmenting and tracking cells in 3d time lapse images. *Elife*, 10:e59187, 2021.
- Michel Couprie and Gilles Bertrand. Topological gray-scale watershed transformation. In *Vision Geometry VI*, volume 3168, pages 136–146. International Society for Optics and Photonics, 1997.
- Özgün Çiçek, Ahmed Abdulkadir, Soeren S Lienkamp, Thomas Brox, and Olaf Ronneberger. 3d u-net: learning dense volumetric segmentation from sparse annotation. In *International conference on medical image computing and computer-assisted intervention*, pages 424–432. Springer, 2016.
- Balázs Szigeti, Padraig Gleeson, Michael Vella, Sergey Khayrulin, Andrey Palyanov, Jim Hokanson, Michael Currie, Matteo Cantarelli, Giovanni Idili, and Stephen Larson. Openworm: an open-science approach to modeling *Caenorhabditis elegans*. *Frontiers in computational neuroscience*, 8:137, 2014.
- Eviatar Yemini, Albert Lin, Amin Nejatbakhsh, Erdem Varol, Ruoxi Sun, Gonzalo E. Mena, Aravinthan D.T. Samuel, Liam Paninski, Vivek Venkatachalam, and Oliver Hobert. Neuropal: A multicolor atlas for whole-brain neuronal identification in *C. elegans*. *Cell*, 184(1):272–288.e11, 2021. ISSN 0092-8674. doi:10.1016/j.cell.2020.12.012.
- Shivesh Chaudhary, Sol Ah Lee, Yueyi Li, Dhaval S Patel, and Hang Lu. Graphical-model framework for automated annotation of cell identities in dense cellular images. *eLife*, 10:e60321, 2021. doi:10.7554/elife.60321.
- Xinwei Yu, Matthew S Creamer, Francesco Randi, Ph.D. Sharma, Anuj Kumar, Scott W Linderman, and Andrew Michael Leifer. Fast deep neural correspondence for tracking and identifying neurons in *C. elegans* using semi-synthetic training. *eLife*, 10:e66410, jul 2021. ISSN 2050-084X. doi:10.7554/eLife.66410. URL <https://doi.org/10.7554/eLife.66410>.

- Jianfeng Cao, Guoye Guan, Vincy Wing Sze Ho, Ming-Kin Wong, Lu-Yan Chan, Chao Tang, Zhongying Zhao, and Hong Yan. Establishment of a morphological atlas of the *caenorhabditis elegans* embryo using deep-learning-based 4d segmentation. *Nature Communications*, 11(1):6254, 2020. doi:10.1038/s41467-020-19863-x.
- Noah F. Greenwald, Geneva Miller, Erick Moen, Alex Kong, Adam Kagel, Christine Camacho Fullaway, Brianna J. McIntosh, Ke Leow, Morgan Sarah Schwartz, Thomas Dougherty, and et al. Whole-cell segmentation of tissue images with human-level performance using large-scale data annotation and deep learning. *bioRxiv*, page 2021.03.01.431313, 2021. doi:10.1101/2021.03.01.431313.
- G. Bradski. The OpenCV Library. *Dr. Dobb's Journal of Software Tools*, 2000.
- Ross Girshick, Jeff Donahue, Trevor Darrell, and Jitendra Malik. Rich feature hierarchies for accurate object detection and semantic segmentation. In *Proceedings of the IEEE conference on computer vision and pattern recognition*, pages 580–587, 2014.
- Ilya Loshchilov and Frank Hutter. Sgdr: Stochastic gradient descent with warm restarts. *arXiv preprint arXiv:1608.03983*, 2016.
- Ashish Vaswani, Noam Shazeer, Niki Parmar, Jakob Uszkoreit, Llion Jones, Aidan N Gomez, Łukasz Kaiser, and Illia Polosukhin. Attention is all you need. In *Advances in neural information processing systems*, pages 5998–6008, 2017.